Characterization of magnetically accelerated flyer plates

R. W. Lemke, M. D. Knudson, C. A. Hall, T. A. Haill, P. M. Desjarlais, J. R. Asay, and T. A. Mehlhorn
Sandia National Laboratories, Albuquerque, New Mexico 87185-1186

(Received 2 October 2002; accepted 19 December 2002)

The intense magnetic field generated by the 20 megaampere Z machine [R. B. Spielman *et al.*, Phys. Plasmas **5**, 2105 (1998)] at Sandia National Laboratories is being used as a pressure source for material science studies. An application we have studied in great detail involves using the intense magnetic field to accelerate flyer plates (small metal disks) to very high velocities (>20 km/s) for use in shock loading experiments. We have used highly accurate velocity interferometry measurements (error ~1%) in conjunction with one-dimensional magnetohydrodynamic (MHD) simulation to elucidate details of the flyer dynamics. One-dimensional MHD simulations are able to produce experimental results with a high degree of accuracy, thereby revealing otherwise unobtainable, but useful information about magnetically accelerated flyers on Z. Comparisons of simulation results with time-resolved measurements of velocity from a shock loading experiment involving a 925 μm aluminum flyer are presented. Results show that Joule heating related to magnetic diffusion constrains the minimum possible initial thickness of a flyer. © *2003 American Institute of Physics.* [DOI: 10.1063/1.1554740]

I. INRODUCTION

The intense magnetic field generated by the Z machine[1] at Sandia National laboratories is being used as a pressure source for material science studies.[2–5] The machine can deliver up to 20 megaamperes (MA) of current to a short-circuited load in 200 nanoseconds (ns), which generates a peak magnetic field in the megagauss (MG) range. An application we have studied in great detail involves using the intense magnetic field to accelerate flyer plates (small metal disks) to very high velocities[6] for use in shock loading experiments. The flyer plate is allowed to collide with a target, which generates a shock in the target material. Measurements of the flyer velocity and the shock speed in the material are used in conjunction with the conservation equations for shocks (i.e., the Rankine–Hugoniot jump conditions)[7] to obtain the density, pressure, and internal energy of the material. In this way, a 1.0 cm diameter, 0.085 cm thick aluminum (Al) flyer plate was accelerated to 21 km/s to obtain state-of-the-art equation of state (EOS) data of deuterium for pressures up to 700 kilobars (kbar).[5]

The shock generated in the target material must remain steady for a sufficient time in order to use the shock conservation equations in conjunction with the measurements to obtain accurate EOS data. This requires that the flyer motion be ballistic at impact. In addition, extraction of EOS data from measurements is simplified if the collision between flyer and target is symmetric. In this case flyer and target materials are identical, which requires that some fraction of flyer material (on the target side) remain at solid density at impact. Whether this can be accomplished or not depends on a number of factors including flyer thickness, material, and current drive. The flyer material is significantly modified by Joule heating associated with the accelerating magnetic field. At impact the flyer may be comprised of solid, liquid, boiling, and plasma regions. The characteristics of the shock (e.g., magnitude and duration) generated in the target are dependent on the condition of the flyer plate at impact, which in turn depends on details of the pressure drive. Hence, it is important to know the state of the flyer when it impacts the target, which cannot be measured explicitly. However, this information in addition to the drive pressure history is contained implicitly in the ensemble of measurements taken in a shock loading experiment,[3,5] and can be extracted from a sufficiently accurate computational analysis of the data. Magnetohydrodynamic (MHD) simulation may provide the most practical way to account for the many coupled, time-dependent, nonlinear phenomena involved.

We present results from one-dimensional (1D) MHD simulations of shock loading experiments that produce the measured velocities with a high degree of accuracy. The excellent agreement between the measured and simulated velocities indicates that the flyer dynamics predicted by the calculations are physically realistic. Detailed comparisons of MHD simulations with experiment confirm that the collision between flyer and target is symmetric for the case investigated, and reveals an accurate density profile for the flyer. In addition, simulations elucidate details of time-dependent phenomena occurring within the flyer (e.g., shock formation, Joule heating, and reverberations) that produce the precise form of the measured velocity.

II. 1-D MHD SIMULATIONS AND COMPARISON WITH EXPERIMENT

A 2D cross section of a typical flyer configuration (shock physics load) used on Z is shown schematically in Fig. 1.[5] The actual geometry is 3D, with a similar cross section in the plane perpendicular to the figure. The magnetic pressure ($P_B = \mathbf{B}^2/2\mu_0$) initiates stress waves in the electrode material

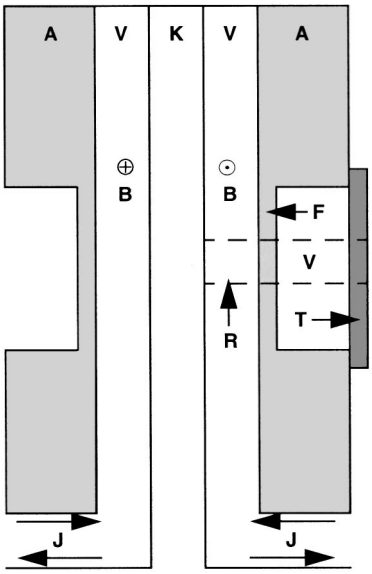

FIG. 1. Cross section of 3D flyer configuration used in shock loading experiments. Anode (A) and cathode (K) are attached in a short circuit at the top of the figure. The flyer (F) is formed by boring out anode material to obtain a desired thickness. The flyer is accelerated across void (V) and impacts a target (T). The directions of the surface current density (**J**) and magnetic field (**B**) are indicated by arrows. A dashed line bounds the 1-D simulation region (R).

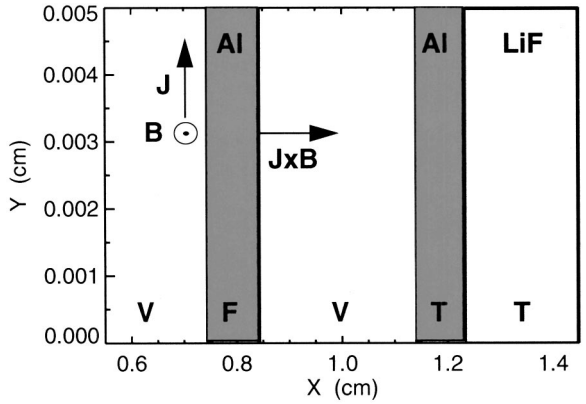

FIG. 2. Schematic of 1D simulation configuration (region R in Fig. 1). The flyer (F) material is Al. The target (T) is comprised of an Al impact plate abutted against a LiF window. The flyer also functions as the anode. The left-hand boundary of the figure is the cathode, which is used to input the driving magnetic field.

that compress the anode (A) and cathode (K). This causes the AK gap [void (V) between the anode and the cathode] to increase. The flyer (F) moves independently of the surrounding anode without losing electrical contact after the initial stress wave releases from the front [target (T)] side of the flyer, and returns to the back (magnetic drive) side. The magnetic force (**J×B**) accelerates the flyer to peak velocity in approximately 0.3 cm, after which time it impacts the target. The region simulated (R) is bounded by the dashed line in Fig. 1.

Measurements indicate that the flyer can become bowed in the plane of Fig. 1 (with ends farther from the target than the center), which could possibly cause important 2D effects. Bowing is caused by nonuniformity in the magnetic pressure across the plane of the flyer, which depends significantly on load geometry. Three-dimensional electromagnetic simulation of a typical load shows that the magnetic field initially varies by less than 0.5% over the central 60% of the flyer surface. In addition, a quantitative measurement of bowing indicates that the central 0.2 cm of a 21 km/s, Al flyer remained planar at impact with the target. This provides the impetus for using 1D simulation to model the problem.

The configuration used for 1D simulations is shown schematically in Fig. 2. As in the experiment, the target (T) is comprised of a 0.1 cm thick Al impact plate abutted against a lithium fluoride (LiF) window. The Al flyer (F) is 0.0925 cm thick. LiF is used for the window in part because it is transparent to the VISAR laser. In addition, the shock impedance (density×shock speed) of LiF is similar to that of Al. Consequently, LiF provides a well-matched interface for shock transmission across the Al/LiF interface (i.e., there is negligible reflection of a shock wave at this surface).

One-dimensional Eulerian simulations were performed using the finite element, arbitrary Lagranagian–Eulerian, MHD code ALEGRA.[8] MHD equations for a compressible material (e.g., see Ref. 9) with strength (e.g., see Ref. 10) were solved. Although the yield strength of Al is approximately 2.8 kilobars (Kbar), strength effects are negligible in this problem because the pressures involved are on the order of megabars (Mbar).

An EOS valid for a wide range of pressures ($P \leqslant 537$ Mbar), densities ($\rho \leqslant 50.0$ g/cm^3) and temperatures ($T \leqslant 1.0 \times 10^5$ Kelvin) was used for Al,[11] in addition to models for the thermal and electrical conductivities.[12] Density and internal energy are used in the EOS to obtain pressure and temperature. The density and temperature are used in the conductivity model to obtain electrical and thermal conductivities. The form of Ohm's law used in ALEGRA is $\vec{J} = \sigma(\vec{E} + \vec{v} \times \vec{B})$, where $\vec{J}$ is the current density, σ the electrical conductivity, $\vec{E}$ the resistive electric field, $\vec{B}$ the applied magnetic field, and $\vec{v}$ the material velocity.

ALEGRA includes artificial viscosity, which broadens shock fronts. To ensure resolution of shocks 50 zones are used across the flyer and 54 across the Al impact plate, with similar resolution in the LiF. One zone is used in the y direction.

The cathode is included only as a fixed conducting boundary (left-hand boundary in Fig. 2) from which to input the magnetic field, which is given by $\mathbf{B} = \mu_0 I(t)/S$. Due to the 1D nature of the simulation, the drive current $[I(t)]$ and the magnetic field scale factor S are free parameters. Nevertheless, a measured waveform was used for $I(t)$, and a value of $S = 4.5$ cm was calculated for the actual experimental configuration using hydrodynamically static, 3D electromagnetic simulation. The drive current measurement is much less accurate than the velocity measurements (10% vs 1%) so slight adjustments were made to the current waveform to produce good agreement with the experiment, thereby determining the actual drive pressure history. The $I(t)$ used in the simulations and corresponding magnetic pressure $[P_B(t)]$ are shown in Fig. 3.

In the experiment, VISAR measurements are used to de-

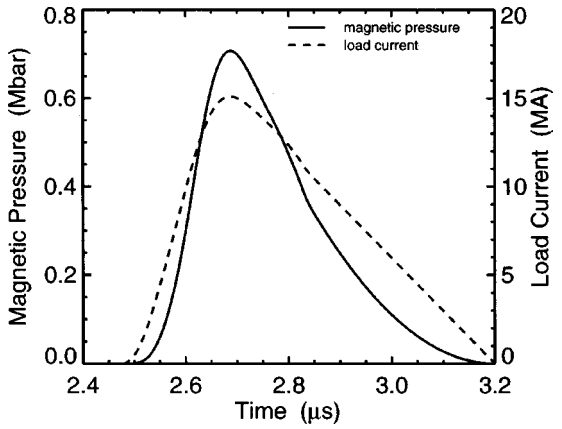

FIG. 3. Current and pressure histories that produce measured flyer plate velocities using 1D MHD simulation.

termine the time-dependent velocities of the flyer (front) surface, and the Al/LiF interface.[3–5] Motion of the Al/LiF interface is induced by passage of the shock generated when the flyer collides with the target. Consequently, the velocity of the Al/LiF interface represents a signature of the collision between flyer and target, and contains time-integrated information pertaining to the spatial profiles of flyer kinetic energy and density at impact. (When the shock pressure is greater than ~1.5 Mbar compression of the LiF window causes it to become opaque, which precludes a measurement of the interface velocity.) The time-dependent flyer velocity contains the integrated pressure drive history. Producing both of these signals with MHD simulation implies that both the pressure (current) drive history and flyer density (in addition to many other quantities) are physically realistic. In fact, if the pressure drive was not known, accurate simulations in conjunction with the velocity measurements could be used to produce it.

Measurements of the flyer surface velocity and Al/LiF interface velocity vs time are compared with simulation results in Figs. 4(a) and 4(b). The measurement error is on the order of 1% for both velocities. The agreement between simulation and experiment is excellent, which provides evidence for the validity of the physics models used in ALEGRA, and implies that the ensemble of simulation results is realistic. In what follows simulation results are used in conjunction with an approximate, but straightforward, analytical analysis to (1) elucidate the phenomena that determine the precise structure of the measured velocity waveforms, and (2) show that the structure of the measured Al/LiF interface velocity implies a symmetric collision.

If the flyer is assumed to be a solid body and magnetic diffusion is slow compared to the acceleration time then the flyer velocity is found by integrating $\rho_0 D(dv/dt)=P_B(t)$, where ρ_0 is the flyer material density, D the flyer thickness, $v(t)$ the velocity, and t the time. Letting $I(t)=I_0 f(t)$ and performing the integration yields

$$v(t)=\frac{\mu_0}{2\rho_0 D}\left(\frac{I_0}{S}\right)^2\int_0^t f(t')^2 dt', \tag{1}$$

where $f(t)$is the time-dependent current waveform in Fig. 3.

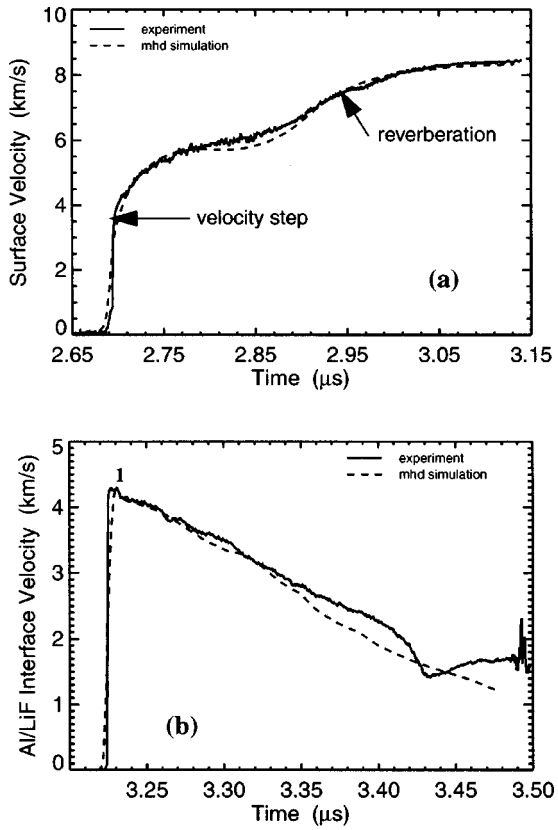

FIG. 4. (a) Comparison of simulated and measured flyer velocity. The initial step in velocity is due to shock formation in the flyer, and is proportional to the peak current. Multiple transits of the pressure wave through the flyer creates a distinct reverberation. (b) Comparison of simulated and measured Al/LiF interface velocity, which is induced through the collision of the flyer with the target. The feature marked by the number 1 is shown in the text to be indicative of a symmetric collision between flyer and target, which implies that some fraction of flyer material remains at solid density at impact. The large kink in the measurement of the Al/LiF interface velocity [at 3.43 μs in Fig. 4(b)] cannot be produced in 1D simulations, and is likely due to release waves that originate at lateral edges of the target and reach the center late in time (i.e., 2D effects).

Equation (1) does not account for details associated with stress wave propagation through the flyer; therefore, it cannot produce the precise structure in the flyer velocity waveform [Fig. 4(a)]. However, under the previous assumptions it does provide an accurate approximation for the final velocity, and shows the correct dependence on the peak current I_0 and magnetic field scale factor S. For the Al flyer at hand, and using the current waveform in Fig. 3, the peak velocity as a function of peak current is given by $v_f=32.7I_0^2$ with I_0 in MA and v_f in m/s. Letting $I_0=15.1$ MA yields $v_f=7.5$ km/s, which is about 12% lower than the measured and simulated values. The difference is due to Joule heating-induced ablation, which increases the flyer velocity on average by 10%–15% in the current range 15–25 MA.

The magnetic pressure applied to the flyer surface induces a stress wave that propagates through the flyer toward the front. For a thick enough flyer the stress wave shocks up and causes a steep initial rise in the flyer velocity when it reaches the front surface. This event occurs at 2.69 μs in Fig. 4(a). For moderately strong shock pressures (~Mbar and greater) an approximate expression for the magnitude of the

velocity step can be derived. In this case an approximate expression for the shock velocity that is consistent with empirical data is given by[7]

$$U_s = a + bu_p, \tag{2}$$

where a is the speed of sound in the uncompressed material, and u_p is the material velocity induced by passage of the shock. For Al, $a=5.35$ km/s and $b=1.34$. An expression for the material velocity is obtained from the jump condition for pressure across the shock front,[7]

$$P = \rho_0 U_s u_p. \tag{3}$$

The form of Eq. (3) is obtained assuming that the pressure behind the shock is much greater than the pressure in front of it, and that the unshocked material velocity is 0. Substituting Eq. (2) into Eq. (3), letting $P=P_B$, and solving for u_p yields

$$u_p = \frac{1}{2b}\left(\sqrt{a^2 + 4b\frac{P_B}{\rho_0}} - a\right). \tag{4}$$

By the conservation of momentum, the shock imparts a velocity to the flyer surface given by $u_s = 2u_p$. For magnetic pressures above a few hundred Kbar, the second term under the radical sign of Eq. (4) is much greater than a. In this case, an approximate expression for the amplitude of the initial step in the flyer surface velocity is given by

$$u_s = \left(\frac{I_0}{S}\right)\sqrt{\frac{2\mu_0}{b\rho_0}} - \frac{a}{b}. \tag{5}$$

Equation (5) shows that for moderately strong shocks the initial step in the flyer surface velocity is proportional to the peak applied current. Using values of 15.1 MA for the peak current and 2.7 g/cm^3 for the density of cold aluminum, Eq. (5) yields $u_s = 4.85$ km/s for the initial step-up in flyer velocity, which is consistent with the measured and simulated results in Fig. 4(a). In this case the maximum magnetic field at the flyer surface is 4.2 MG, which yields $P_B = 0.7$ Mbar for the peak drive pressure.

The shock that causes the initial jump in the flyer surface velocity must reflect from this surface in a way that keeps the total pressure equal to 0 (the void pressure). This generates a rarefaction (release) wave that propagates with the Lagrangian sound speed U_r through the compressed material toward the back (drive side) of the flyer. U_r is related to the hydrodynamic pressure and material velocity[7] as follows: $\rho_0 U_r = dP/du_p$. Using Eqs. (2) and (3) in the previous expression yields

$$U_r = a + 2bu_p, \tag{6}$$

for the speed of the release wave. When the latter reaches the drive side a new stress wave whose magnitude is determined by the value of the magnetic field at that time is generated and moves into the flyer. Hence, when the rise time of the current waveform is on the order of the round trip transit time for the initial compression and release waves, $D(1/U_s + 1/U_r)$, a reverberation of significant amplitude can occur, resulting in a second step in velocity and recompression of the flyer. This is exemplified in Fig. 4(a).

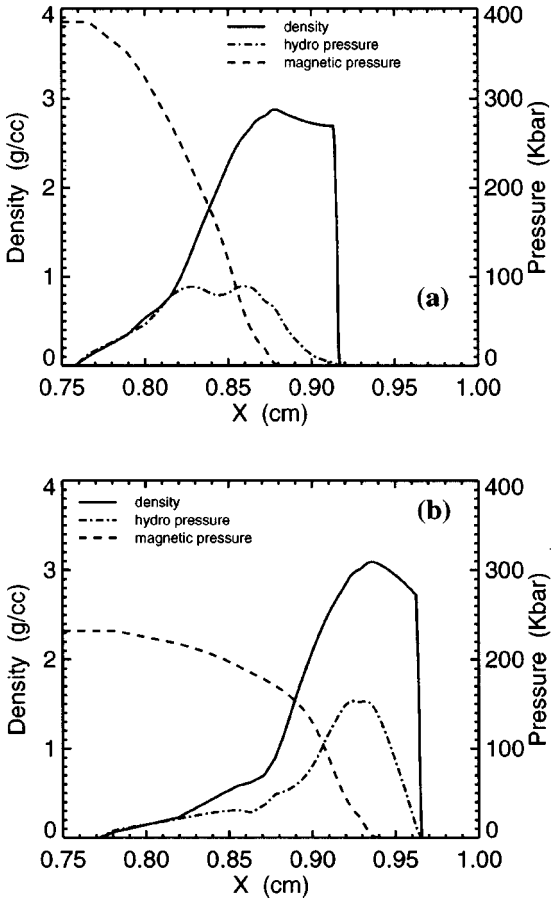

FIG. 5. Snapshots of flyer density, magnetic pressure, and hydrodynamic pressure at (a) time=2.83 μs, and (b) time=2.91 μs. In (a) the release wave has reduced the pressure at the drive surface to a local minimum, which occurs at $X_0=0.84$ cm. The reverberation wave originates at X_0, and its peak amplitude is determined by the value of the magnetic field at this location. The fully developed wave is shown in (b).

The flyer density, magnetic pressure, and hydrodynamic pressure are plotted as functions of position in Fig. 5 for two stages of the reverberation. The flyer material is evidently significantly modified at these times due to the combination of Joule heating and compression. Figure 5(a) is a snapshot at $t=2.83$ μs, which corresponds to the time that the release wave has reduced the pressure at the magnetic boundary to its minimum value. This creates a local minimum in the pressure that is evident in Fig. 5(a) at position $X_0 \sim 0.84$ cm. The total pressure is dominated by magnetic to the left of X_0 and hydrodynamic to the right of it. X_0 defines the boundary at which the recompression (reverberation) wave is launched. The amplitude of the recompression wave is determined by the value of the magnetic pressure at X_0, which is why it has been referred to as the magnetic boundary. For the case at hand $P_B \sim 150$ Kbar. The recompression wave reaches its peak amplitude ($P \sim 150$ kbar) at $t=2.91$ μs. Conditions at this time are shown in Fig. 5(b). The front of the recompression wave is at the flyer surface and is starting to increase its velocity. This is evident in Fig. 4(a).

From the standpoint of pressure wave propagation, X_0 defines the effective back surface of the flyer and determines an effective thickness D_{eff}, which may not correspond to the

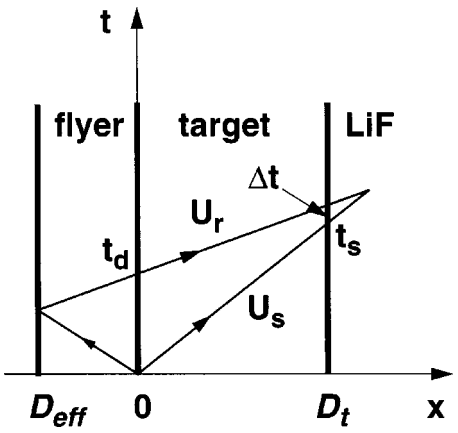

FIG. 6. Graphical illustration of collision between flyer and target in a Lagrangian reference frame whose origin ($x=0$) is at the impact plane. Target and flyer are assumed to be A1. The duration of constant pressure at $x=0$ is the dwell time (t_d). Shock waves emanate from $x=0$ and move into the target and flyer with speed U_s. The shock wave in the flyer releases at location D_{eff}. The resulting rarefaction wave moves toward the Al/LiF interface with Lagrangian sound speed U_r, which is greater than U_s. As shown, the two waves merge in the LiF. When the shock transits the Al/LiF interface (at time t_s) it induces a velocity to the right that remains constant for a time Δt until the rarefaction wave catches up to it. The shock impedance of LiF is similar to that of Al; therefore it is assumed that reflections at the Al/LiF interface are negligible. The velocity measurements in Fig. 4 provide values for Δt and the magnitude of the constant interface velocity. These are used to assess whether or not the collision is symmetric and to calculate D_{eff}.

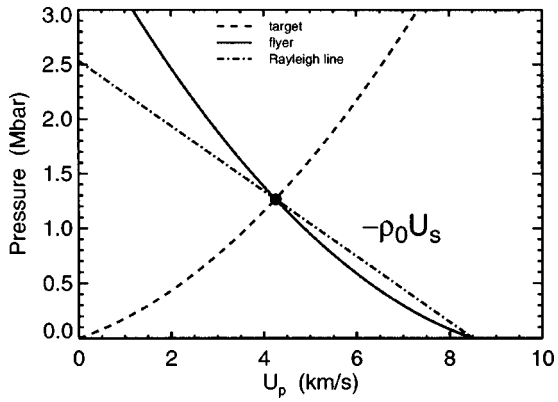

FIG. 7. Graphical illustration of a symmetric collision between A1 flyer and A1 target using shock Hugoniots. Shock pressure is plotted vs material velocity. The collision causes the flyer material to slow down and target material to speed up by exactly one-half the flyer velocity at impact. The Rayleigh line connects the initial and final states and the slope $|\rho_0 U_s|$. The latter indicates how the post-collision pressure and material velocity depends on material density and shock speed.

thickness of flyer material at solid density. In what follows it is shown that (1) D_{eff} corresponds to the distance behind the front of the flyer where pressure waves reflect (the magnetic boundary) or release, and (2) D_{eff} corresponds to the actual flyer thickness only when the entire flyer remains at solid density ($\rho_0 = 2.7$ g/cm^3) at impact. A graphical illustration of the collision between flyer and target is used to obtain an expression for D_{eff}. The analysis is used in conjunction with the measurements in Fig. 4 to estimate D_{eff}, and to show that some fraction of the flyer must remain at solid density when it collides with the target.

The dynamics of the collision between flyer and target are illustrated graphically in Fig. 6, which depicts the collision in a Lagrangian frame of reference whose origin is at the impact plane. It is assumed that the collision is symmetric; that is, flyer and target materials are identical. At the moment of impact, shocks are generated at the impact plane that move into both flyer and target with speed U_s. The shock in the flyer unloads at the location D_{eff}, which generates a rarefaction wave that moves with Lagrangian sound speed U_r in the direction of the LiF window. Equations (2) and (6) show that $U_s < U_r$; consequently, the rarefaction wave eventually catches up to the shock moving through the target. After this occurs the shock is unsteady. In Fig. 6 it is assumed that the shock and rarefaction waves merge in the LiF.

As is shown in Fig. 6, when the shock crosses the Al/LiF interface (at time t_s) the latter moves to the right with constant velocity (the material velocity u_p) for a time Δt until the rarefaction wave catches up to it. Knowledge of u_p and Δt can be used to determine D_{eff}. Let t_d represent the duration (dwell time) of the collision at the target–flyer interface, and let $D_t (= 0.1$ cm) denote the target thickness. It is clear from Fig. 6 that $t_d + D_t/U_r = t_s + \Delta t, t_d = D_{\text{eff}}(1/U_s + 1/U_r)$, and $t_s = D_t/U_s$. Combining these equations yields

$$D_{\text{eff}} = D_t \frac{(U_r - U_s)}{(U_r + U_s)} + \Delta t \frac{U_s U_r}{(U_r + U_s)}, \tag{7}$$

with U_s and U_r given as functions of u_p by Eqs. (2) and (6), respectively. The material velocity (u_p) and Δt can be obtained from the measurements shown in Fig. 4.

In a symmetric collision the material velocity (u_p) induced by the resulting shocks can be obtained graphically by plotting the Hugoniots for both flyer and target. The latter are obtained by substituting Eq. (2) into Eq. (3), which yields

$$P_{\text{H}} = \rho_0 (a + b u_p) u_p . \tag{8}$$

Equation (8) expresses the relationship between material velocity and pressure behind a shock front, and is plotted in Fig. 7 for both the Al flyer and A1 target. The flyer velocity at impact time is the peak velocity in Fig. 4(a), ~8.5 km/s. The intersection of the Hugoniots marks the impact point, which gives the shock pressure and material velocity associated with the collision; these are, respectively, ~1.3 Mbar and $u_p = 4.25$ km/s. Evidently the material velocity induced in a symmetric collision is exactly one-half the velocity of the impactor. (Figure 7 shows that this cannot be true if the density of material at the front of the flyer is not solid.) Using the previous value of u_p in Eqs. (2) and (6) yields $U_s = 11.04$ km/s and $U_r = 16.74$ km/s.

The time Δt is obtained from a measurement of the Al/LiF interface velocity [Fig. 4(b)]. We clarify this with a less complicated simulation problem in which a constant velocity, Al flyer undergoes a symmetric collision with a target identical to that of the experiment. The geometry is exactly like that shown in Fig. 2, but there is no magnetic drive. In the absence of a magnetic field the flyer thickness at impact is well defined, and can be controlled. The constant flyer velocity is 8.5 km/s, which is equal to the impact velocity mea-

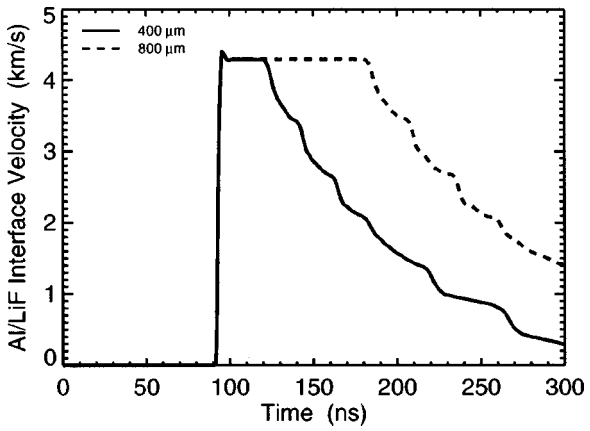

FIG. 8. A plot of simulated Al/LiF interface velocity vs time for the simplified problem in which a solid density, Al flyer with constant velocity 8.5 km/s undergoes a symmetric collision with an Al/LiF target. The configuration is identical to that of Fig. 2, but there is no magnetic field involved so the entire flyer remains solid until impact. Interface velocities are plotted for flyer thicknesses of 400 and 800 μm. In each case the interface velocity rises to approximately one-half the flyer velocity and remains constant for a time Δt, which is indicative of a symmetric collision. The time Δt evidently decreases with decreasing flyer thickness. In the 400 μm case $\Delta t \sim 28.04$ ns, and $\Delta t \sim 88.53$ ns in the 800 μm case.

sured in the magnetically accelerated flyer experiment [Fig. 4(a)]. To determine the effect of flyer thickness on Δt, thickness of 400 and 800 μm were used. The resulting interface velocities for these two cases are plotted vs time in Fig. 8. The time Δt evidently decreases with decreasing flyer thickness. In the 400 μm case $\Delta t \sim 28.04$ ns, and in the 800 μm case $\Delta t \sim 88.53$ ns. Using these values of Δt, and the previous values for U_s and U_r in Eq. (7) yields $D_{\text{eff}} = 391$ μm and $D_{\text{eff}} = 794$ μm, which are in good agreement with the actual flyer thicknesses used in the two cases. Hence, in the case of a solid density, constant velocity flyer Eq. (7) provides an accurate estimate of the actual flyer thickness.

Returning to the case of the magnetically accelerated Al flyer plate, inspection of Fig. 4(b) shows that the measured interface velocity initially rises to ~4.25 km/s, which is one-half of the peak flyer velocity, and remains at this value for ~6.5 ns. Therefore, the collision is symmetric and some fraction of the flyer plate was at solid density when it impacted the Al target. Substituting $\Delta t \sim 6.5$ ns, and the previous values for U_s and U_r in Eq. (7) yields $D_{\text{eff}} = 248$ μm. In this case, D_{eff} can be compared with an accurate flyer density profile at impact determined by simulation, which shows that the previous value of D_{eff} is greater than the thickness of solid density material.

Figure 9 shows a snapshot of the simulated flyer density vs position just before it impacts the Al part of the target ($t = 3.1$ μs) in the magnetically driven problem. The temperature and magnetic field in the flyer are superimposed on the plot of density in Figs. 9(a) and 9(b), respectively. Noting that Al melts and boils at temperatures of 933 and 2723 K, respectively, it is evident from Fig. 9(a) that at impact the flyer consists of solid, liquid, boiling, and vaporized regions of A1. These phase transitions are marked by the numbers 1 (solid–liquid), 2 (liquid–boiling), and 3 (boiling–vapor). It is clear from the figure that approximately 140 μm (0.014

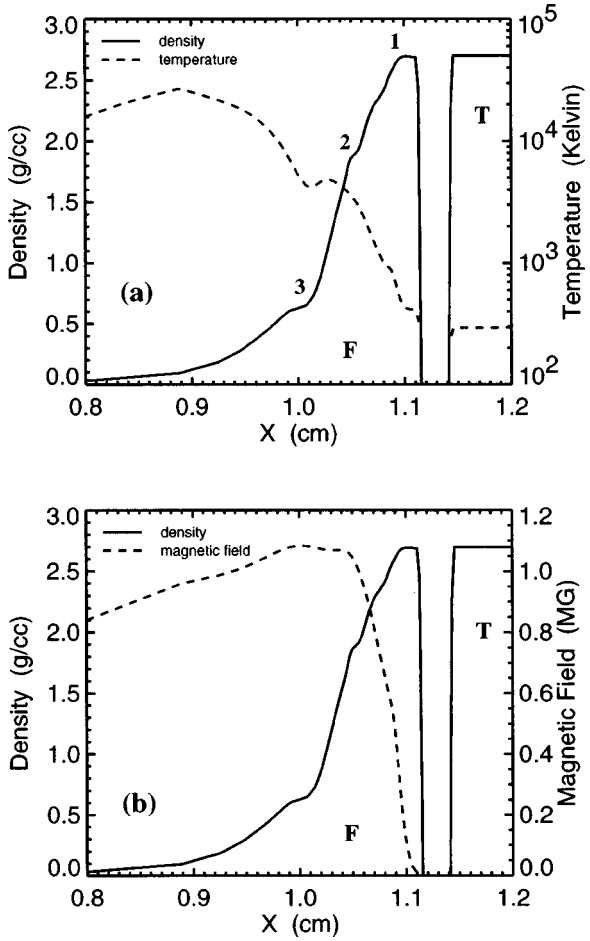

FIG. 9. Snapshots of simulated density and temperature (a), and density and magnetic field (b) in the Al flyer (F) just before it impacts the target (T). Using the known values of the melting and boiling temperatures of Al, the location of solid–liquid and liquid–boiling phase transitions can be determined. In addition, the decrease in temperature at $x = 1.01$ cm indicates the boiling–vapor/plasma transition. These phase transitions are marked in (a) using the numbers 1, 2, and 3, respectively. On the target side, approximately 140 μm (0.014 cm) of the flyer material is in the solid state (density $= 2.7$ g/cm^3). (b) shows that the solid–liquid transition marks the point in the flyer to which significant magnetic fields has diffused.

cm or 15%) of flyer material remains at solid density, which is consistent with the interpretation of the velocity measurements in Fig. 4 (i.e., collision was symmetric). However, in contrast to the solid density, constant velocity flyer problem, the calculated value of $D_{\text{eff}} = 248$ μm is much greater than the thickness of solid Al at impact, which implies that the unloading boundary (see Fig. 6) is in the liquid region of the flyer (density $= 2.56$ g/cm^3), 108 μm behind the solid–liquid transition.

A side effect of using magnetic pressure to accelerate a metallic flyer plate to high velocity is that Joule heating associated with diffusion of the magnetic field into the flyer substantially heats the material, thereby producing a layered flyer comprised of solid, liquid, boiling, and vaporized regions, as shown in Fig. 9(a). The solid–liquid transition marks the point to which significant magnetic field has diffused into the flyer. Comparisons of Figs. 9(a) and 9(b) show that the material temperature in the flyer increases to ~30 000 K behind the location of the solid–liquid transition,

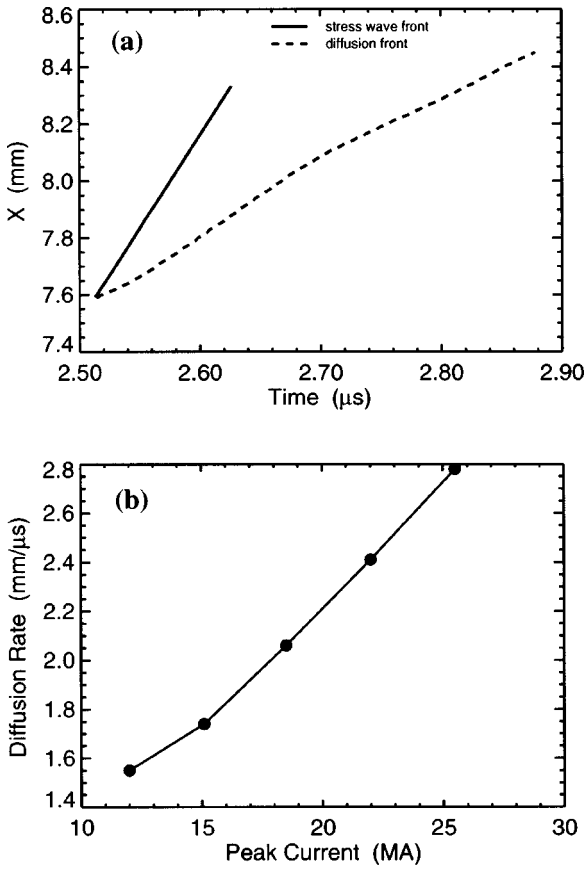

FIG. 10. (a) Locations of hydrodynamic pressure wave and magnetic diffusion front vs time in a Lagrangian reference frame of a 0.0925 cm thick Al flyer (i.e., relative to an observer that is stationary with respect to the flyer). Results were obtained using a peak drive current of 22.0 MA. Evidently the accelerating pressure wave moves into the flyer faster than the diffusion front. (b) Diffusion rate vs peak drive current showing a linear relationship between these parameters for peak currents in the range $15 \leqslant I_0 \leqslant 25$ MA. The diffusion rate is the slope of a straight line fit to the location of the diffusion front vs time for each current.

which is well correlated with increasing values of the magnetic field. If the flyer is too thin, or the acceleration time too long, Joule heating can destroy the entire flyer. Hence, the magnetic diffusion rate constrains the minimum flyer thickness, which can be quantified using simulation results.

One-dimensional simulations in which the peak current (I_0) was varied up to a maximum value of 25.5 MA show that the stress wave induced in the Al flyer is faster than the magnetic diffusion rate (R_B) in general. This is illustrated in Fig. 10(a) for $I_0 = 22.0$ MA. Figure 10(a) is a plot of the location of the stress wave and magnetic diffusion fronts in a Lagrangian frame of reference attached to a 925 μm thick Al flyer. Hence, the velocity with which these fronts move toward the front of the flyer are relative to an observer that is stationary in the flyer. A pressure of 1 Kbar was used to mark the front of the stress wave, and a magnetic field of 2 KG defined the diffusion front. The stress wave is tracked until just before it reaches the front surface of the flyer. The diffusion front is followed until just before the flyer collides with the target. The velocity of the stress wave is clearly greater than the diffusion rate, which guarantees that Joule heating does not destroy the flyer before it starts to move.

An average diffusion rate (R_B) for the duration of a current pulse is defined as the slope of a straight line fit to the location of the diffusion front vs time for a given peak current. Figure 10(b) is a plot of R_B vs I_0 for peak currents in the range $12 \leqslant I_0 \leqslant 25.5$ MA. The diffusion rate evidently increases linearly with peak drive current in the range $15 \leqslant I_0 \leqslant 25.5$ MA. For peak currents in this range $R_B = 0.10 I_0 + 0.22$ (mm/μs), where I_0 is in MA. To ensure that the flyer arrives at the target with some material unaffected by the magnetic field, the initial flyer thickness (D) must be greater than $D_{\min} = R_B t_a$, where t_a is the time it takes to accelerate the flyer to the target. Alternatively, magnetic diffusion places a requirement on t_a for a given D.

The desired accuracy of the VISAR measurement, which depends on the dwell time (t_d) of the collision, puts an additional constraint on $D_{\min}$. Let $t_{d\min}$ represent the minimum dwell time that achieves a certain measurement accuracy. Then the minimum initial thickness of flyer material that ensures measurement accuracy and accounts for the effect of Joule heating is given approximately by

$$D_{\min} = \frac{U_s U_r}{(U_s + U_r)} t_{d\min} + R_B t_a . \tag{9}$$

Equation (9) shows that $D_{\min}$ is determined by material properties, experimental accuracy, and Joule heating effects. As an example, we estimate the value of $D_{\min}$ required to accelerate an Al flyer to 20 km/s over a 0.3 cm gap using a peak current of 21.5 MA, and achieve a measurement accuracy of $\approx$1%. The diffusion rate for this current [Fig. 10(b)] is 2.35 mm/μs. Using an average velocity of 15 km/s across the gap (obtained from a related simulation with $S = 3.65$ cm) yields $t_a = 200$ ns. Typically, $t_{d\min} \sim 30$ ns for the desired accuracy. The shock physics considerations discussed above are used to get $U_s = 18.75$ km/s and $U_r = 32.15$ km/s. Substituting the appropriate values into Eq. (9) yields $D_{\min} = 0.0825$ cm (825 μm). Fifty-seven percent of this thickness is used to prevent significant levels of magnetic field from diffusing into the front 43% of the flyer during the acceleration time.

III. DISCUSSION AND CONCLUSIONS

Given an accurate current to drive the problem, the ability of 1D MHD simulations to accurately produce the experimental results contained herein depends on whether or not the relevant physics models have been included, and on the fidelity of those models. Our initial 1D simulations could not produce both of the measured velocities in Fig. 4 simultaneously (i.e., one or the other would be different from the measurement by a significant amount). Research indicated that the simulated velocity waveforms are particularly sensitive to the behavior of the electrical conductivity that a given model produces at the metal–insulator transition in the flyer material (e.g., aluminum).

The model of Lee and More (which contains extensive physics)[13] yields a large value (factor of 2 above measured value) of electrical conductivity for solid A1, which persisted through the metal–insulator transition. This resulted in a slow diffusion rate, a lower flyer velocity in general (relative

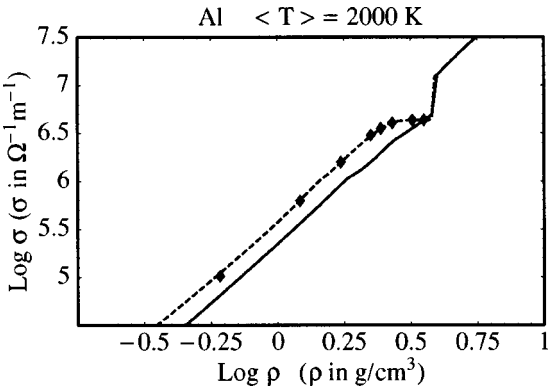

FIG. 11. A comparison of electrical conductivity vs density at temperature 2000 K, as obtained from quantum QMD simulation (dashed line with symbols), and the LMD model (solid line). The vertical step marks the melt transition. Simulations that used the QMD conductivity model accurately produce both measured velocities in Fig. 4.

to measurements), and too much Al at solid density at impact with the target. A model based on Lee–More (called LMD[14]) that accurately fit measurements of Al electrical conductivity in the solid and expanded (warm, dense) regimes produced low values of electrical conductivity after the metal–insulator transition. This resulted in flyers that were, at best, completely melted at impact with the target, in contrast to what velocity measurements indicated.

Quantum molecular dynamics (QMD) simulations based on density functional theory were used to investigate the behavior of the electrical conductivity of dense liquid aluminum.[12] As is shown in Fig. 11 for Al at a temperature of 2000 K, the QMD model yields larger values of electrical conductivity after the metal–insulator transition than does the aforementioned LMD model. Simulations that used the QMD corrected model of electrical conductivity proved to be the most accurate.

One-dimensional MHD simulations of shock loading experiments that employed the QMD corrected model of electrical conductivity produced the measured velocities with a high degree of accuracy. The excellent agreement between the measured and simulated velocities indicates that the flyer dynamics predicted by the calculations are physically realistic. Detailed comparisons of MHD simulation with experiment confirm that the collision between flyer and target is symmetric for the case investigated, and reveals an accurate density profile for the flyer. Analysis shows that this results in steady shock generation, which validates the use of conservation equations for shocks in determining EOS data from velocity measurements. Furthermore, simulation results show that the accelerating magnetic field does not completely burn through the flyer, thereby rendering it useless for EOS experiments. It was shown that magnetic diffusion constrains the minimum initial thickness of the flyer, which must increase as peak current is increased to obtain ultrahigh velocities (>20 km/s) without Joule heating destroying the entire flyer. In addition, simulations show that the precise form of the measured flyer velocity is determined by details of time-dependent phenomena occurring within the flyer, such as shock formation, Joule heating, and reverberations.

ACKNOWLEDGMENTS

The authors would like to thank D. B. Hayes for insightful discussions.

Sandia National Laboratories is a multiprogram laboratory operated by Sandia Corporation, a Lockheed Martin Company, for the U.S. Department of Energy under Contract No. DE-AC04-94AL85000.

[1] R. B. Spielman, C. Deeney, G. A. Chandler, M. R. Douglas, D. L. Fehl, M. K. Matzen, D. H. McDaniel, T. J. Nash, J. L. Porter, T. W. L. Sanford, J. F. Seaman, W. A. Stygar, K. W. Struve, S. P. Breeze, J. S. McGurn, J. A. Torres, D. M. Zagar, T. L. Gilliland, D. O. Jobe, J. L. McKenney, R. C. Mock, M. Vargas, T. Wagoner, and D. L. Peterson, Phys. Plasmas **5**, 2105 (1998).

[2] J. R. Asay, *Shock Compression of Condensed Matter—1999*, edited by M. D. Furnish, L. C. Chhabildas, and R. X. Hixson (American Institute of Physics, Melville, 2000), p. 261.

[3] C. A. Hall, J. R. Asay, M. D. Knudson, W. A. Stygar, R. B. Spielman, T. D. Pointon, D. B. Reisman, A. Toor, and R. C. Cauble, Rev. Sci. Instrum. **72**, 3587 (2001).

[4] D. B. Reisman, A. Toor, R. C. Cauble, C. A. Hall, J. R. Asay, M. D. Knudson, and M. D. Furnish, J. Appl. Phys. **89**, 1625 (2001).

[5] M. D. Knudson, D. L. Hanson, J. E. Bailey, C. A. Hall, J. R. Asay, and W. W. Anderson, Phys. Rev. Lett. **87**, 225501 (2001).

[6] H. Knoepfel, *Pulsed High Magnetic Fields* (North Holland, London, 1970), pp. 116–122.

[7] A. V. Bushman, G. I. Kanel, A. L. Ni, and V. E. Fortov, *Intense Dynamic Loading of Condensed Matter* (Taylor and Francis, Washington, DC, 1993), p. 6.

[8] R. M. Summers, J. S. Peerey, M. W. Wong, E. S. Hertel, Jr., T. G. Trucano, and L. C. Chhabildas, Int. J. Impact Eng. **20**, 779 (1997).

[9] L. D. Landau and E. M. Lifshitz, *Electrodynamics of Continuous Media* (Pergamon, New York, 1960), pp. 213–217.

[10] A. V. Bushman, G. I. Kanel, A. L. Ni, and V. E. Fortov, *Intense Dynamic Loading of Condensed Matter* (Taylor and Francis, Washington, DC, 1993), pp. 1–12 and pp. 34–46.

[11] G. I. Kerley (private communication, 2000).

[12] M. P. Desjarlais, J. D. Kress, and L. A. Collins, Phys. Rev. E **66**, 025401(R) (2002).

[13] Y. T. Lee and R. M. More, Phys. Fluids **27**, 1273 (1984).

[14] M. P. Desjarlais, Contrib. Plasma Phys. **41**, 267 (2001).